

1 Article

## 2 Fatigue assessment of prestressed concrete slab- 3 between-girder bridges

4 Eva O.L. Lantsoght<sup>1,2,\*</sup>, Rutger Koekkoek<sup>3</sup>, Cor van der Veen<sup>4</sup> and Henk Sliedrech<sup>5</sup>

5 <sup>1</sup> Politécnico, Universidad San Francisco de Quito, Quito, Ecuador; elantsoght@usfq.edu.ec

6 <sup>2</sup> Concrete Structures, Delft University of Technology, Delft, the Netherlands; [E.O.L.Lantsoght@tudelft.nl](mailto:E.O.L.Lantsoght@tudelft.nl)

7 <sup>3</sup> BAM Infraconsult, Gouda, the Netherlands; [rutger.koekkoek@bam.com](mailto:rutger.koekkoek@bam.com)

8 <sup>4</sup> Concrete Structures, Delft University of Technology, Delft, the Netherlands; [C.vanderveen@tudelft.nl](mailto:C.vanderveen@tudelft.nl)

9 <sup>5</sup> Rijkswaterstaat, Ministry of Infrastructure and the Environment, Utrecht, the Netherlands;

10 [henk.sliedrech@rws.nl](mailto:henk.sliedrech@rws.nl)

11 \* Correspondence: [elantsoght@usfq.edu.ec](mailto:elantsoght@usfq.edu.ec); Tel.: (+593) 2 297-1700 ext. 1186

12 Received: date; Accepted: date; Published: date

13 **Featured Application:** The results of this work can be used for the evaluation of existing prestressed  
14 concrete slab-between-girder bridges for fatigue.

15 **Abstract:** In the Netherlands, the assessment of existing prestressed concrete slab-between-girder  
16 bridges showed that the thin, transversely prestressed slabs may be critical for static and fatigue  
17 punching when evaluated using the recently introduced Eurocodes. On the other hand, compressive  
18 membrane action increases the capacity of these slabs and changes the failure mode from bending  
19 to punching shear. To improve the assessment of the existing prestressed slab-between-girder  
20 bridges in the Netherlands, two 1:2 scale models of an existing bridge, the Van Brienenoord Bridge,  
21 were built in the laboratory and tested monotonically as well as under cycles of loading. The result  
22 of these experiments is: 1) the static strength of the decks, showing that compressive membrane  
23 action significantly enhances the punching capacity, and 2) the Wöhler curve of the decks, showing  
24 that compressive membrane action remains under fatigue loading. The experimental results can  
25 then be used for the assessment of the most critical existing slab-between-girder bridge. The  
26 outcome is that the bridge has sufficient punching capacity for static and fatigue loads, and thus  
27 that the existing slab-between-girder bridges in the Netherlands fulfil the code requirements for  
28 static and fatigue punching.

29 **Keywords:** Assessment; Bridge evaluation; Compressive membrane action; Concrete bridges;  
30 Fatigue; Fatigue assessment; Live loads; Prestressed concrete; Punching shear; Scale model.

### 32 1. Introduction

33 The majority of the bridges in the Dutch highway bridge stock were built in the decades  
34 following World War II, which was an era of rapid and extensive expansion of the Dutch road  
35 network. These bridges were designed for the live loads of that era, which resulted in lower demands  
36 on the bridges than the recently introduced Eurocode live loads from NEN-EN 1991-2:2003 [1]. In  
37 terms of capacity, the design capacities for shear and punching from the previously used Dutch codes  
38 (e.g. VBC 1995 – NEN 6723 [2]) are larger than those determined using the recently introduced  
39 Eurocode for concrete structures NEN-EN 1992-1-1:2005 [3]. With higher demands and lower  
40 capacities according to the Eurocodes, the outcome of an assessment is often that existing bridges do  
41 not fulfil the code requirements for brittle failure modes such as shear [4] and punching [5]. This  
42 problem is not limited to the Netherlands; similar discussions take place in Germany [6], Sweden [7],  
43 Switzerland [8], and other European countries, as well as in the United States [9], where bridge  
44 construction peaked in the 1930s (the New Deal) and between 1956 and 1992 (construction of the  
45 Interstate Highway System). As one can see, methods for an accurate assessment of existing bridges

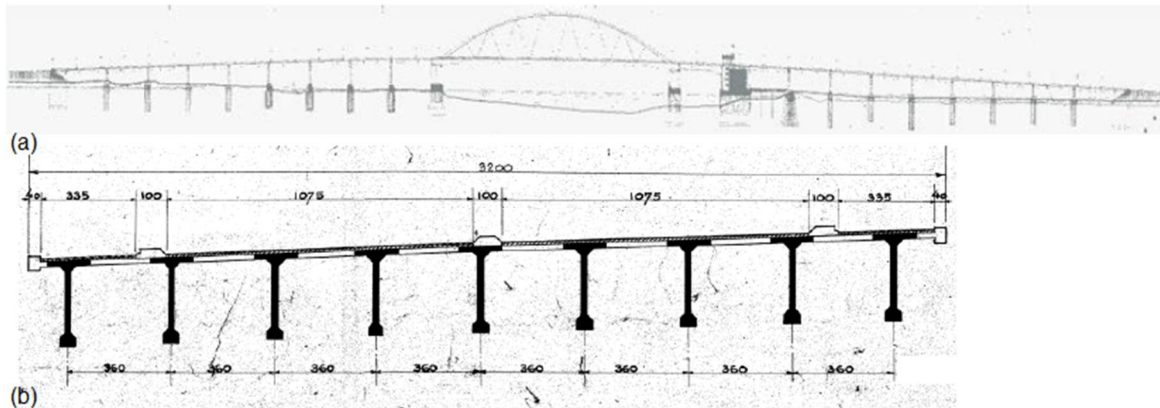
46 are becoming increasingly important, as the safety of the traveling public should be protected, and at  
47 the same time, unnecessary bridge replacement or strengthening actions should be avoided [10].

The preliminary assessment of the existing bridges in the Netherlands according to the new Eurocodes was based on hand calculations (Quick Scans [11,12]), and categories of bridge types that require further study were identified. One such category contains prestressed slab-between-girder bridges. This subset contains about 70 bridges [5]. The structural system of these bridges is a combination of prestressed girders with the deck slab cast in between the girders and transversely prestressed. As a result, the top of the flange of the girders is flush with the top of the deck. Additionally, prestressed diaphragm beams provide stiffness to the overall system. Upon assessment, the thin deck slabs do not fulfil the code requirements for punching shear. One mechanism that is not considered in the codes, but that enhances the capacity of these thin decks, is compressive membrane action [13-20]. Additionally, the fatigue capacity of the thin decks is subject to discussion, as it is not known if progressive cracking and damage accumulation affects the capacity-enhancing effect of compressive membrane action [21].

60 This work summarizes experimental results from testing 1:2 scale models of prestressed slab-  
61 between-girder bridges, and then applies these results to the punching and fatigue assessment of an  
62 existing bridge. We show how compressive membrane action improves the assessment for punching  
63 shear, and how the Wöhler curve from the fatigue tests can be used for the assessment of the bridge  
64 deck under fatigue. The summarized experiments are unique in nature, as the tested specimens give  
65 us insight in the behavior of slab-between-girder bridges as a structural system. Most fatigue testing  
66 in the past focused on testing small specimens [22,23] or structural elements [24-31] instead of  
67 structural systems. The insights from these experiments are now reported for the first time in the  
68 context of bridge assessment. This analysis shows that, based on the experimental evidence, it is  
69 found that the existing slab-between-girder bridges in the Netherlands fulfil the safety requirements  
70 of the code, and in particular the requirements for punching shear under static and fatigue live  
71 loading.

## 72 2. Materials and Methods

### 73 2.1. Description of case study bridge



75 **Figure 1.** Van Brienenoord Bridge: (a) sketch of elevation of entire bridge structure, showing approach  
 76 slabs as well as steel arch; (b) cross-section of the slab-between-girder approach bridge. Dimensions  
 77 in cm.

78 Of the 70 slab-between-girder bridges in the Netherlands, the one that has the most critical slab  
 79 geometry (largest span to depth ratio of  $3.6\text{ m} / 0.2\text{ m} = 18$ ) is the approach bridge of the Van  
 80 Brienenoord Bridge in Rotterdam, see **Figure 1a**. The approach spans are 50 m in length and consist  
 81 of thin, transversely post-tensioned decks cast in between simply supported post-tensioned girders,  
 82 see **Figure 1b** [13]. The clear span of the slab is 2100 mm. The transverse prestressing level is 2.5 MPa.  
 83 The duct spacing in the deck is 650 mm on center, and at some positions it is increased to 800 mm on  
 84 center. **Table 1** gives the main properties of the geometry and reinforcement of the decks. Post-

85 tensioned crossbeams are built at the end of the spans and post-tensioned diaphragm beams are  
 86 provided at 1/3 and 2/3 of the span length.

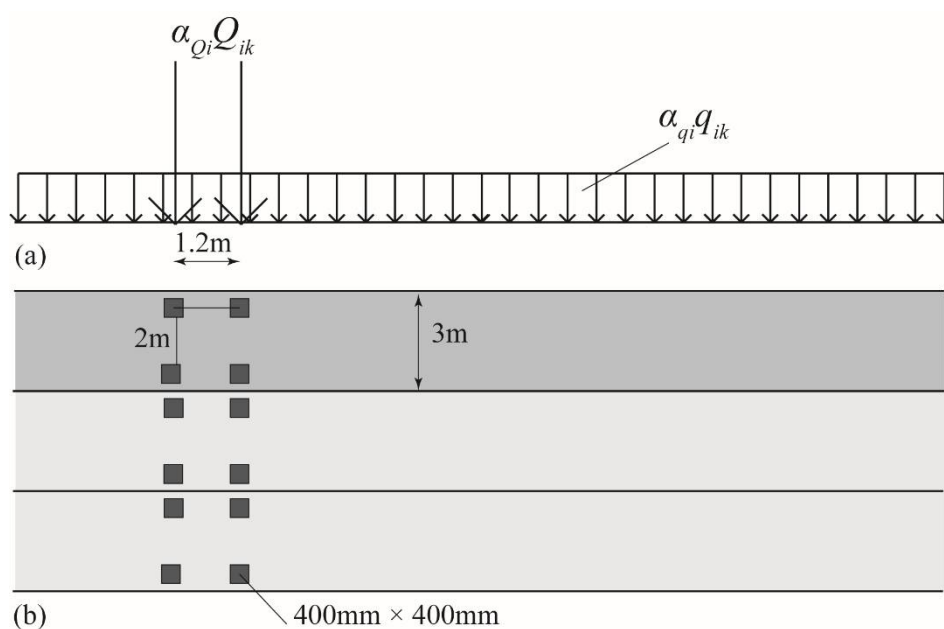
87 At the time of construction, the design concrete compressive strength of the deck was B35 ( $f_{ck,cube}$   
 88 = 35 MPa) and of the girders B45 ( $f_{ck,cube} = 45$  MPa). Testing of cores taken from the deck slab resulted  
 89 in an average  $f_{cm,cube} = 98.8$  MPa ( $f_{ck,cube} = 84.6$  MPa) as a result of the continued cement hydration. For  
 90 the assessment calculations, it is conservatively assumed that the mean compressive cylinder strength  
 91  $f_{cm} = 65$  MPa in the deck. The associated characteristic concrete compressive strength is  $f_{ck} = 53$  MPa.

92 **Table 1:** Main properties of geometry and reinforcement of decks of Van Brienenoord Bridge.

Dimension	Value
Thickness $h$	200 mm
Concrete cover $c$	30 mm
Longitudinal reinforcement	$\phi 8$ mm – 250 mm
Effective depth longitudinal $d_l$	166 mm
Area of longitudinal reinforcement $A_{s,l}$	201.1 mm <sup>2</sup> /m
Longitudinal reinforcement ratio $\rho_l$	0.12%
Transverse reinforcement	$\phi 8$ mm – 200 mm
Effective depth transverse $d_t$	158 mm
Area of transverse reinforcement $A_{s,t}$	251.3 mm <sup>2</sup> /m
Transverse reinforcement ratio $\rho_t$	0.16%
Average effective depth $d$	162 mm
Average reinforcement ratio $\rho_{avg}$	0.14%
Prestressing reinforcement	462 mm <sup>2</sup> – 800 mm
Area of prestressing steel $A_{sp}$	0.5775 mm <sup>2</sup> /mm

93 **2.2. Live load models**

94 Two live load models are relevant for the assessment of the Van Brienenoord Bridge: Load  
 95 Model 1 for the assessment of the punching capacity, and Fatigue Load Model 1 for the fatigue  
 96 assessment, both from NEN-EN 1991-2:2003 [1].



99 **Figure 2.** Live Load Model 1 from NEN-EN 1991-2:2003 [1]: (a) elevation; (b) top view. Edited from  
 100 [12], reprinted with permission.

101 Live Load Model 1 combines a distributed lane load with a design tandem. The design tandem  
 102 has the following characteristics: 1) wheel print of 400 mm  $\times$  400 mm, 2) axle distance of 1.2 m, and  
 103 3) transverse spacing between wheels of 2 m. The magnitude of the axle load is  $\alpha_{Q1} \times 300$  kN in the  
 104 first lane,  $\alpha_{Q2} \times 200$  kN in the second lane, and  $\alpha_{Q3} \times 300$  kN in the third lane [12]. For the Netherlands,  
 105 the values of all  $\alpha_{Qi} = 1$  with  $i = 1 \dots 3$ . The uniformly distributed load acts over the full width of the  
 106 notional lane of 3 m wide, and equals  $\alpha_{q1} \times 9$  kN/m<sup>2</sup> for the first lane, and  $\alpha_{qi} \times 2.5$  kN/m<sup>2</sup> for all other  
 107 lanes. For bridges with three or more notional lanes in the Netherlands, the value of  $\alpha_{q1} = 1.15$  and  $\alpha_{qi} = 1.4$  with  $i > 1$ . **Figure 2** shows a sketch of live Load Model 1.

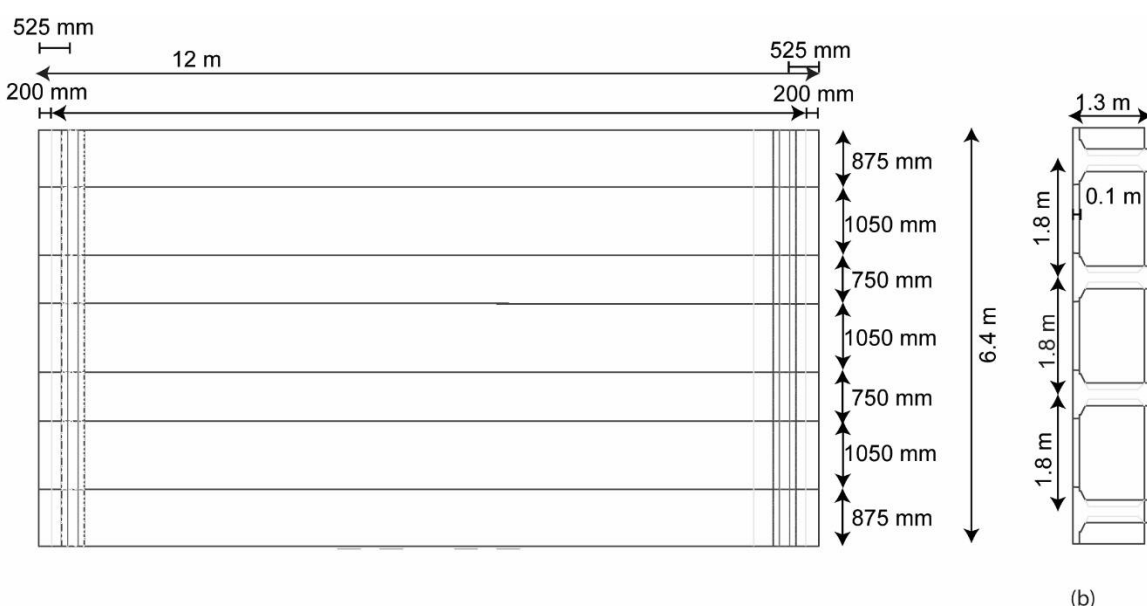
109 Fatigue Load Model 1 has the same configuration as Load Model 1, with  $0.7Q_{ik}$  for the axle loads  
 110 and  $0.3q_{ik}$  for the distributed lane loads. In other words, the axle load becomes  $0.7 \times 300$  kN = 210 kN,  
 111 and the load per wheel print becomes 105 kN. The distributed lane load is  $0.3 \times 1.15 \times 9$  kN/m<sup>2</sup> = 3.105  
 112 kN/m<sup>2</sup>. The fatigue load model has as a reference load 2 million trucks per year. In the Netherlands,  
 113 the guidelines for the assessment of bridges (RBK [32]) use a higher number of passages: 2.5 million  
 114 trucks per year. Over a lifespan of 100 years, the result is 250 million truck passages.

115 In the Netherlands, assessment is carried out both with a wheel print of 400 mm  $\times$  400 mm (as  
 116 prescribed by the Eurocode 1 NEN-EN 1991-2:2003 [1]) and of 230 mm  $\times$  300 mm (used for the fatigue  
 117 evaluation of joints, but often used as an additional check in assessment as well).

### 118 2.3. Description of experiments

119 Two 1:2 scale models of an existing bridge were built in the laboratory and tested monotonically  
 120 as well as under cycles of loading. Full descriptions of the first series of static tests [5,13], first series  
 121 of fatigue tests [33-35], and second series of fatigue tests [36,37] can be found elsewhere. The  
 122 description in this paper is limited to the information necessary for interpreting the test results for  
 123 the application to assessment of the case study bridge.

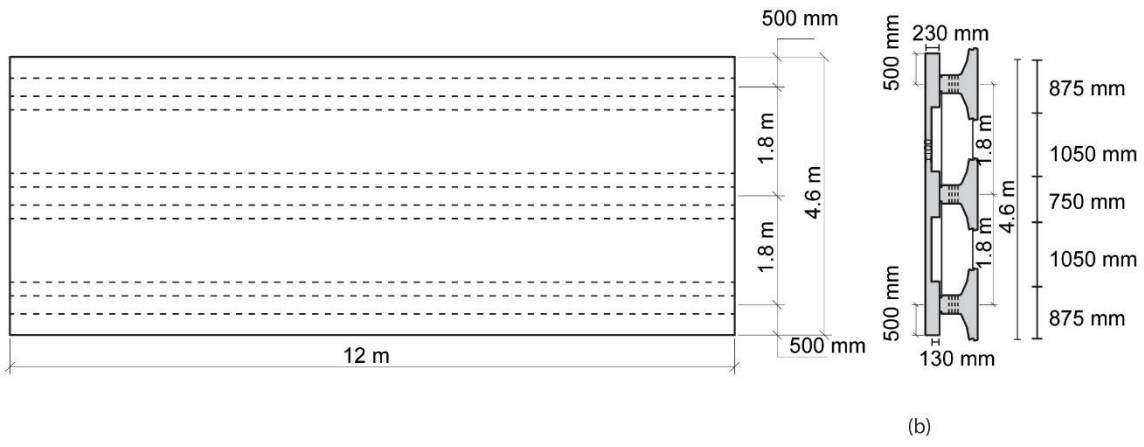
124 The first 1:2 scale model (6.4 m  $\times$  12 m, see **Figure 3**) used four prestressed concrete T-girders  
 125 with a center-to-center spacing of 1.8 m, length  $l = 10.95$  m, and height  $h = 1.3$  m; two post-tensioned  
 126 crossbeams ( $b = 350$  mm,  $h = 810$  mm), and three transversely post-tensioned decks with  $h = 100$  mm  
 127 and  $b = 1050$  mm between the girders. The post-tensioning of the deck was applied through  
 128 prestressing bars placed in 30 ducts of diameter 40 mm, spaced 400 mm apart. To increase the number  
 129 of experiments that could be carried out on this scale model, the middle deck was removed after  
 130 testing and a new deck was cast. One segment of the new deck contained ducts of diameter 30 mm,  
 131 spaced 300 mm apart to study the influence of the duct spacing.



132 (a)

133 **Figure 3.** Dimensions of first 1:2 scale model: (a) top view; (b) cross-section view. Figure adapted from  
 134 [34]. This figure was originally published in Vol. 116 of the ACI Structural Journal.

135 The second 1:2 scale model (4.6 m × 12 m, see **Figure 4**) used three prestressed concrete bulb T-  
 136 girders and two post-tensioned decks. The dimensions of the girders, crossbeams, and decks are the  
 137 same as for the first 1:2 scale model, with the exception of the shape of the girders (T-girders in the  
 138 first scale model and bulb T-girders in the second scale model). For the second scale model, the top  
 139 flange of the girders was cast in the laboratory, monolithically with the deck. The advantage of this  
 140 approach is that the weight of the girders is reduced, which facilitates transportation and handling.



141 (a) (b)  
 142 **Figure 4.** Overview of second 1:2 scale setup: (a) top view; (b) cross-section view. Figure adapted from  
 143 [37]. This figure was originally published in Vol. 116 of the ACI Structural Journal.

144 Standard cube specimens are used for determining the concrete compressive strength for the  
 145 concrete of the different casts. The results for the 28 days strength are as follows:  $f_{cm,cube} = 75$  MPa for  
 146 the original slab in setup 1,  $f_{cm,cube} = 68$  MPa for the newly cast slab in setup 1,  $f_{cm,cube} = 81$  MPa for the  
 147 first cast of setup 2, and  $f_{cm,cube} = 79$  MPa for the second cast of setup 2.

148 Mild steel reinforcement is used for the longitudinal and transverse reinforcement in the deck  
 149 slabs. In setup 1, the longitudinal reinforcement is  $\phi = 6$  mm at 200 mm o.c. top and bottom, and the  
 150 transverse reinforcement is  $\phi = 6$  mm at 250 mm o.c. top and bottom. In setup 2, the longitudinal  
 151 reinforcement is  $\phi = 8$  mm at 200 mm o.c. top and bottom, and the transverse reinforcement is  $\phi = 8$   
 152 mm at 240 mm o.c. top and bottom. The clear cover to the reinforcement is 7 mm. The mild steel  
 153 reinforcement in the setups is B500B steel, except for the bars of 6 mm diameter, for which B500A  
 154 steel was used. Stress-strain curves of the mild steel for all bar diameter are measured in the  
 155 laboratory, see [33,36].

156 The prestressing steel in the girders is Y1860S tendons and the prestressing steel in the  
 157 crossbeams and slabs is Y1100H prestressing bars with a diameter of 15 mm. The transverse  
 158 prestressing in the deck results in an axial compressive stress of 2.5 MPa.

159 The size of the concentrated load in the experiments is 200 mm × 200 mm for the experiments on  
 160 the original first setup, which is 1:2 scale of the wheel print of 400 mm × 400 mm from the design  
 161 tandem of Load Model 1 in NEN-EN 1991-2:2003 [1]. For all other experiments, the size of the loading  
 162 plate was 115 mm × 150 mm, or 1:2 scale the wheel print of 230 mm × 300 mm used for the assessment  
 163 in the Netherlands of bridge joints for fatigue.

164 The load is applied with a hydraulic jack mounted in a steel frame test setup. For the static tests,  
 165 the load is applied with a stepwise monotonic loading protocol. In two experiments, a loading  
 166 protocol with three cycles per load levels is used. For the static tests and the tests with three cycles  
 167 per load level, the load is applied in a displacement-controlled way. For the fatigue tests, the load is  
 168 cycled between a lower limit and upper limit, with the lower limit 10% of the upper limit. A sine  
 169 function is used with a frequency of 1 Hz. The load is applied in a force-controlled way for the fatigue  
 170 tests. If fatigue failure does not occur after a large number of cycles, the upper load level is increased  
 171 (and the associated lower limit of 10% of the upper limit adjusted as well) and fatigue testing is  
 172 continued.

173 **3. Results**174 *3.1. Results of experiments*

175 The complete results of all experiments can be consulted in [5] for the static tests on the first  
 176 setup, in [34] for the fatigue tests on the first setup, and in [37] for the tests on the second setup. Here,  
 177 only the results that are relevant for the assessment of the case study bridge are summarized.

178 **Table 2** gives an overview of the relevant static tests from the first setup (BB tests) and second  
 179 setup (FAT tests). For the BB series, all experiments are numbered consecutively. For the FAT series,  
 180 the test number gives information about the experiment: FAT (fatigue testing series of experiments  
 181 on setup 2), followed by the test number, and then S (static test) or D (dynamic test), and 1 (load  
 182 applied through one loading plate representing a single wheel load) or 2 (load applied through two  
 183 loading plates representing a double wheel load). The tables gives the size of the loading plate used  
 184 for testing, the load at failure  $P_{max}$ , the age of the concrete of the slab at the moment of testing, and the  
 185 concrete cube compressive strength  $f_{cm,cube}$  determined at the day of testing the slab.

186 **Table 2.** Overview of static tests used for assessment of case study bridge

Test number	Size load (mm × mm)	$P_{max}$ (kN)	Age (days)	$f_{cm,cube}$ (MPa)
BB1	200 × 200	348.7	96	80.0
BB2	200 × 200	321.4	99	79.7
BB7	200 × 200	345.9	127	80.8
BB19	200 × 200	317.8	223	79.9
FAT1S1	150 × 115	347.8	94	82.2
FAT7S1	150 × 115	393.7	240	88.8
FAT8S2	2 of 150 × 115	646.1	245	88.6

187 **Table 3** gives an overview of the fatigue tests. Here, all tests are considered relevant for the  
 188 fatigue assessment, since all fatigue tests are used to derive the Wöhler curves. The test number is  
 189 given, with BB the experiments on the first setup and FAT the experiments on the second setup. Then,  
 190 the number of the setup is listed, with “1, new” for the experiments that were carried out on the  
 191 newly cast deck in the first setup. Next, the size of the loading plate used for applying the load on the  
 192 slab is reported, followed by “Wheel”, which can be S (single wheel print) or D (double wheel print).  
 193 Then, the upper load level used in the test,  $F/P_{max}$  (with  $P_{max}$  from a static test) is given, as well as  $N$ ,  
 194 the number of cycles. For the variable amplitude fatigue tests,  $N$  is the number of cycles for the  
 195 associated load level  $F/P_{max}$ . After  $N$  cycles at load level  $F/P_{max}$ , given on one row of **Table 3**, the test  
 196 is continued with  $N$  cycles at another load level  $F/P_{max}$ , given on the next row. The column “Age”  
 197 gives the age of the slab at the age of testing, and  $f_{cm,cube}$  gives the associated cube concrete compressive  
 198 strength. For fatigue tests that lasted several days, a range of ages is given in the column “Age”,  
 199 indicating the age of the concrete in the slab at the beginning of testing and at the end of testing.  
 200 Similarly, a range of compressive strengths is given for  $f_{cm,cube}$ , representing the strength determined  
 201 at the beginning and end of testing.

203 **Table 3.** Overview of punching fatigue experiments

Test Number	Setup	Size load (mm × mm)	Wheel	$F/P_{max}$	N	Age (days)	$f_{cm,cube}$ (MPa)
BB17	1	200 × 200	S	0.80	13	147	82.6
BB18	1	200 × 200	S	0.85	16	56	82.6
BB23	1	200 × 200	S	0.60	24,800	301	79.9
BB24	1	200 × 200	S	0.45	1,500,000	307-326	79.9
BB26	1, new	150 × 115	S	0.48	1,405,337	35-59	70.5-76.7
BB28	1, new	150 × 115	S	0.48	1,500,000	68-97	76.8-77.1

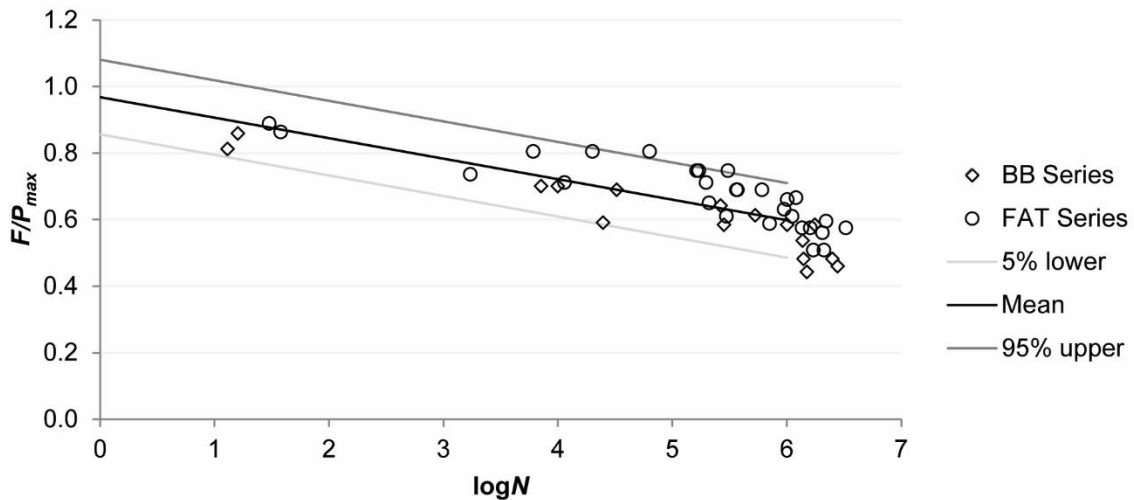
					0.58	1,000,000	97-113	77.1-77.3
					0.70	7144	113	77.3
BB29	1, new	150 × 115	S	0.58	1,500,000	117-136	77.3-77.5	
				0.64	264,840	136-139	77.5-77.6	
BB30	1, new	150 × 115	D	0.58	100,000	143-144	77.6	
				0.50	1,400,000	144-162	77.6-77.8	
				0.58	750,000	162-171	77.8-77.9	
				0.67	500,000	171-177	77.9-78.0	
				0.75	32,643	177	78.0	
BB32	1, new	150 × 115	S	0.70	10,000	184	78.1	
				0.58	272,548	185-187	78.1	
FAT2D1	2	150 × 115	S	0.69	100,000	102-144	82.6-84.6	
				0.58	2,915,123			
				0.69	100,000			
				0.75	150,000			
				0.81	20,094			
FAT3D1	2	150 × 115	S	0.69	200,000	149-168	84.9-85.8	
				0.58	1,000,000			
				0.69	100,000			
				0.75	300,000			
				0.81	6114			
FAT4D1	2	150 × 115	S	0.58	1,000,000	169-190	85.8-86.8	
				0.69	200,000			
				0.75	100,000			
				0.81	63,473			
FAT5D1	2	150 × 115	S	0.71	10,000	192-217	91.6-89.6	
				0.51	1,000,000			
				0.61	100,000			
				0.66	1,000,000			
				0.71	1424			
FAT6D1	2	150 × 115	S	0.71	10,000	219-239	89.6-88.8	
				0.51	1,000,000			
				0.61	100,000			
				0.71	160,000			
				0.51	410,000			
				0.71	26,865			
FAT9D2	2	150 × 115	D	0.59	500,000	246-255	88.5-88.2	
				0.65	209,800			
FAT10D2	2	150 × 115	D	0.63	100,000	260-284	90.2-91.3	
				0.56	1,000,000			
				0.63	950,928			
FAT11D2	2	150 × 115	D	0.67	100,000	288-315	91.5-92.8	
				0.60	1,000,000			
				0.67	1,100,000			
				0.75	1720			
FAT12D1	2	150 × 115	S	0.89	30	318	85.9	
FAT13D1	2	150 × 115	S	0.86	38	319	85.8	

204 3.2. Resulting Wöhler curve

205 To find the Wöhler curve of the fatigue experiments, the relation between the logarithm of the  
 206 number of cycles  $N$  and the applied load ratio  $F/P_{max}$  is plotted, see Figure 5. The variable amplitude  
 207 loading tests are interpreted as follows for this curve: if  $N_1$  cycles at load level  $F_1$  are applied, followed

208 by  $N_2$  cycles at  $F_2$ , and then  $N_3$  cycles to failure at  $F_3$ , with increasing load levels  $F_1 < F_2 < F_3$ , it is then  
 209 conservative to assume that the slab can withstand  $N_1 + N_2 + N_3$  cycles at load level  $F_1$ ,  $N_2 + N_3$  cycles  
 210 at load level  $F_2$ , and  $N_3$  cycles at load level  $F_3$ . This approach leads to three datapoints for one variable  
 211 amplitude fatigue test. As a result of this approach, we obtained 16 datapoints on the first setup and  
 212 28 datapoints on the second setup, resulting in the 44 datapoints in **Figure 5**. The average value of  
 213 the Wöhler curve is shown as “Mean” in **Figure 5** and is described with the following expression,  
 214 using  $S$  for the load ratio and  $N$  for the number of cycles to failure:

215 
$$S = -0.062 \log N + 0.969 \quad (1)$$



216  
 217 **Figure 5.** Relation between number of cycles  $N$  and applied load ratio  $F/P_{max}$  in all fatigue experiments,  
 218 from [37]. Reprinted with permission. This figure was originally published in Vol. 116 of the ACI  
 219 Structural Journal.

220 Since the assessment will be carried out separately for one and two wheel prints, it is interesting  
 221 to look at the difference in Wöhler curve for the experiments with one and two wheel prints. **Figure**  
 222 **6** gives these results, with the datapoints from the FAT series for a single wheel print in **Figure 6a**  
 223 and the datapoints for a double wheel print in **Figure 6b**. The markers in **Figure 6** are different for  
 224 the datapoints obtained at a number of cycles that results in failure and a number of cycles that was  
 225 calculated with the conservative assumption mentioned previously. The Wöhler curve for the  
 226 datapoints with a single wheel load is:

227 
$$S = -0.066 \log N + 1.026 \quad (2)$$

228 The 5% lower bound (characteristic value) of this expression, which can be used for assessment, is:

229 
$$S_{char} = -0.066 \log N + 0.922 \quad (3)$$

230 The Wöhler curve for the datapoints with a double wheel load is:

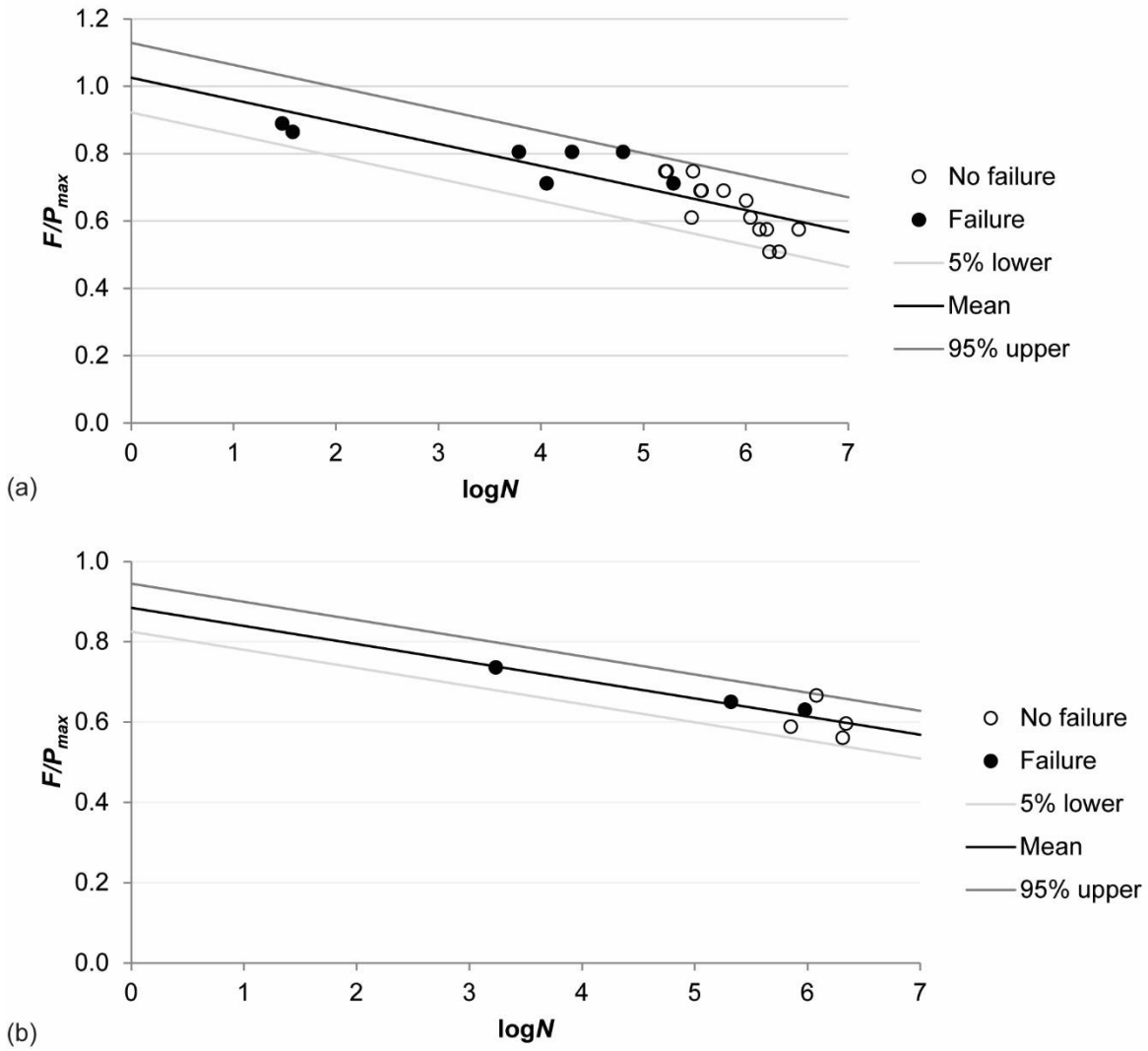
231 
$$S = -0.045 \log N + 0.885 \quad (4)$$

232 The 5% lower bound of this expression is:

233 
$$S_{char} = -0.045 \log N + 0.825 \quad (5)$$

234 The slope of the Wöhler curve for the case with two wheel loads is lower than for the case with a  
 235 single wheel load. However, for the case with a double wheel load, no low-cycle fatigue experimental  
 236 results are available. For one load cycle Eq. (2) gives a load ratio of 1.026 and for Eq. (4) this value  
 237 is 0.885. The difference between the two Wöhler curves for one cycle is significant. However, for 1  
 238 million load cycles, Eq. (2) gives a load ratio of 0.63 and Eq. (4) a load ratio of 0.62. For a large number

239 of load cycles, the difference between the two Wöhler curves thus becomes smaller. It is the large  
 240 number of cycles that need to be considered for the assessment of existing bridges.



241

242 **Figure 6.** Relation between number of cycles  $N$  and applied load level  $F/P_{max}$  for (a) a single wheel  
 243 load; and (b) a double wheel load, from [37]. Reprinted with permission. This figure was originally  
 244 published in Vol. 116 of the ACI Structural Journal.

245 *3.3. Assessment of case study bridge for punching*

246 First, the capacity of the thin slab for punching is evaluated based on the experimental results.  
 247 The shear capacity according to NEN-EN 1992-1-1:2005 [3] is calculated:

$$248 \quad v_{Rd,c} = C_{Rd,c} k \left( 100 \rho_{avg} f_{ck} \right)^{1/3} + k_1 \sigma_{cp} \geq v_{min} + k_1 \sigma_{cp} \quad (6)$$

249 with

$$250 \quad k = 1 + \sqrt{\frac{200 \text{mm}}{d}} \leq 2 \quad (7)$$

251 and

$$252 \quad \rho_{avg} = \sqrt{\rho_l \times \rho_t} \quad (8)$$

$$253 \quad \sigma_{cp} = \frac{\sigma_{cx} + \sigma_{cy}}{2} \quad (9)$$

254 The recommended value for  $k_1 = 0.1$ , for  $C_{Rd,c} = 0.18/\gamma_c$  with  $\gamma_c = 1.5$  and for  $v_{\min}$ :

255 
$$v_{\min} = 0.035k^{3/2} \sqrt{f_{ck}} \quad (10)$$

256 Using the properties in **Table 1**, we find that  $k = 2$  and the punching shear stress capacity of the case  
257 study bridge equals:

258 
$$v_{Rd,c} = \frac{0.18}{1.5} \times 2 \times (100 \times 0.001388 \times 53.3 \text{ MPa})^{1/3} + 0.1 \times 1.25 \text{ MPa} = 0.572 \text{ MPa} \quad (11)$$

259 To find the maximum punching force, we calculate the punching perimeter around the 400 mm wheel  
260 print as sketched in Figure 7:

261 
$$u = 4 \times 400 \text{ mm} + 2\pi \times 2 \times 162 \text{ mm} = 3636 \text{ mm} \quad (12)$$

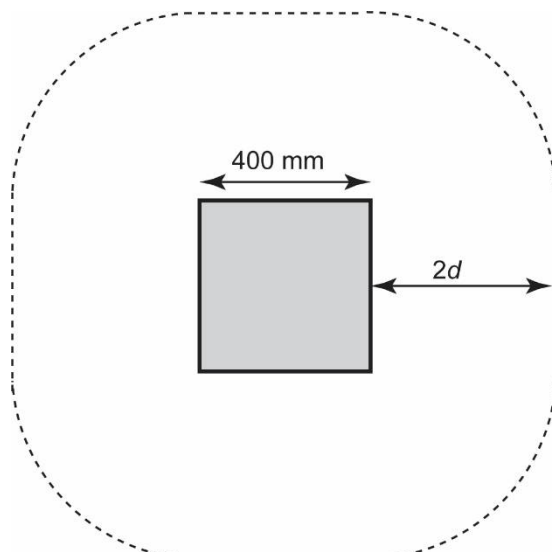
262 For the 230 mm  $\times$  300 mm wheel print, the punching perimeter length becomes:

263 
$$u = 2 \times (230 \text{ mm} + 300 \text{ mm}) + 2\pi \times 2 \times 162 \text{ mm} = 3096 \text{ mm} \quad (13)$$

264 The maximum punching force for these two wheel prints then becomes:

265 
$$V_{Rd,c} = 0.572 \text{ MPa} \times 3636 \text{ mm} \times 162 \text{ mm} = 336.8 \text{ kN} \quad (14)$$

266 
$$V_{Rd,c} = 0.572 \text{ MPa} \times 3096 \text{ mm} \times 162 \text{ mm} = 286.8 \text{ kN} \quad (15)$$



267

268 **Figure 7.** Punching perimeter around wheel print

269 The load that the deck has to resist is a combination of the concentrated live load and distributed  
270 live load. The axle load of 300 kN results in a wheel load of 150 kN. The distributed lane load is  $1.15$   
271  $\times 9 \text{ kN/m}^2 = 10.35 \text{ kN/m}^2$ . The contributions of the self-weight and asphalt are respectively  $25 \text{ kN/m}^3$   
272  $\times 200 \text{ mm} = 5 \text{ kN/m}^2$  and  $23 \text{ kN/m}^3 \times 120 \text{ mm} = 2.8 \text{ kN/m}^2$ . The area over which these loads are  
273 considered is the area within the punching perimeter,  $A_u = (400 \text{ mm})^2 + 4 \times 162 \text{ mm} \times 400 \text{ mm} +$   
274  $\pi(162 \text{ mm}/2)^2 = 439,812 \text{ mm}^2 = 0.4398 \text{ m}^2$ . The corresponding loads for the distributed lane load, self-  
275 weight, and asphalt then become 4.55 kN, 2.2 kN, and 1.23 kN when the Eurocode wheel print is  
276 considered. For the smaller wheel print, the area within the punching perimeter becomes  $A_u = 0.2613$   
277  $\text{m}^2$ , resulting in loads of 2.7 kN, 1.3 kN, and 0.7 kN respectively for the distributed lane load, the self-  
278 weight, and the asphalt.

279 The load combination for the assessment of existing bridges in the Netherlands depends on the  
280 required safety level, as prescribed by NEN 8700:2011 [38] and the RBK (Guidelines for the  
281 Assessment of Existing Bridges) [32]. The highest level is the “Design” level (associated reliability  
282 index  $\beta = 4.3$ ), which gives the following load combination:  $U = 1.25DL + 1.25DW + 1.50LL$ , with  $DL$

283 the dead load,  $DW$  the superimposed dead load, and  $LL$  the live load. The resulting factored  
 284 concentrated load for evaluation then becomes 236 kN for the 400 mm  $\times$  400 mm wheel print and 232  
 285 kN for the 230 mm  $\times$  300 mm wheel print.

286 The assessment is carried out based on the Unity Check. The Unity Check is the ratio of design  
 287 demand to design capacity; for punching in this case, the Unity Check is the ratio of the factored  
 288 concentrated load acting on the wheel print to the design punching shear force capacity. To fulfil the  
 289 code requirements, the Unity Check has to be smaller than 1. **Table 4** gives an overview of the  
 290 resulting Unity Checks for the different wheel prints studied. It can be seen that assessing the deck  
 291 with the Eurocode already fulfils the requirements. In the introduction, we stated that there is  
 292 discussion about the punching capacity of the decks in the existing slab-between-girder bridges. The  
 293 reason why this assessment already shows that the deck fulfils the code requirements is the higher  
 294 punching capacity that is found based on the results of drilled cores.

295 **Table 4.** Overview of resulting Unity Check according to Eurocode

Wheel print	$V_{Ed}$ (kN)	$V_{Rd,c}$ (kN)	Unity Check
400 mm $\times$ 400 mm	236	337	0.70
230 mm $\times$ 300 mm	232	287	0.81

296  
 297 In a next step of the assessment, the maximum loads obtained in the static tests are applied to  
 298 the assessment of the Van Brienenoord Bridge. When assessing the bridge based on the results of the  
 299 experiments, we can replace the design capacity according to the Eurocode  $V_{Rd,c}$  with the capacity  
 300 obtained in the tests. To translate the capacity obtained in the test to a representative design capacity  
 301 of the case study bridge, we have to consider the following (see Annex D of NEN-EN 1990:2002 [39]):

- 302 • the laboratory setup is 1:2 scale of the case study bridge, resulting in a factor 2<sup>2</sup>;
- 303 • considering scaling laws, a scale factor of 1.2 [13] has to be included on the capacity;
- 304 • the partial factor derived from the experiments  $\gamma_T$  has to be included.

305 First, we will derive the partial factor from the experiments  $\gamma_T$ . To calculate this factor, we compare  
 306 the punching capacity obtained in the static experiments with the average punching stress capacity  
 307  $v_{R,c}$  according to NEN-EN 1992-1-1:2005 [3]. The expression for  $v_{R,c}$  is given in the background report  
 308 of Eurocode 2 [40] as follows:

$$309 \quad v_{R,c} = 0.18 \times k \times (100 \times \rho_{avg} \times f_{cm})^{1/3} + 0.08 \sigma_{cp} \quad (16)$$

310 To find the punching shear capacity  $V_{R,c}$  the stress  $v_{R,c}$  is then multiplied with  $u \times d$ , with  $u$  determined  
 311 as in **Figure 7** for the considered wheel print. **Table 5** then combines the experimental results  $V_{exp}$  and  
 312 the predicted capacities  $V_{R,c}$ , as well as the ratio of tested to predicted capacity  $V_{exp}/V_{R,c}$ . The average  
 313 value of  $V_{exp}/V_{R,c}$  is 2.61, with a standard deviation of 0.296 and coefficient of variation of 11%. This  
 314 information then leads to the derivation of  $\gamma_T$  as determined in Annex C of NEN-EN 1990:2002 [39]:

$$315 \quad \gamma_T = \frac{\mu}{B_{Rd}} \quad (17)$$

316 with

$$317 \quad B_{Rd} = \mu (1 - \alpha \times \beta \times COV) = 2.61 (1 - 0.8 \times 4.3 \times 0.11) = 1.622 \quad (18)$$

318 with  $\alpha = 0.8$  the factor for considering experimental results and  $\beta$  the target reliability index. The value  
 319 for  $\gamma_T$  then becomes:

$$320 \quad \gamma_T = \frac{\mu}{B_{Rd}} = \frac{2.61}{1.622} = 1.61 \quad (19)$$

321 As for the influence of the difference in scale between the test setup in the laboratory and the  
 322 case study bridge, the experimental result  $V_{exp}$  can be scaled to the capacity of the bridge  $V_{BB}$  as  
 323 follows:

324

$$V_{BB} = V_{exp} \times \frac{2^2}{1.2} \quad (20)$$

325 where the factor 2<sup>2</sup> corrects for the 1:2 scale and 1.2 is the scaling factor. The design capacity  
326 based on the test results is then:

327

$$V_{BB,d} = \frac{V_{BB}}{\gamma_T} \quad (21)$$

328 **Table 6** shows the results for  $V_{BB}$  according to Eq. (20) and  $V_{BB,d}$  according to Eq. (21), as well as the  
329 demand  $V_{Ed}$  that corresponds to the wheel print in the experiment under consideration (see **Table 4**).  
330 The average value of  $V_{BB,d}/V_{Ed} = 3.06$ , which means that the margin of safety is 3.23, or that the Unity  
331 Check is the inverse,  $UC = 0.33$ . When comparing this value based on the experiments to the values  
332 in **Table 4**, we can observe the beneficial effect of compressive membrane action on the capacity of  
333 thin transversely prestressed concrete slabs.

334 **Table 5.** Comparison between mean predicted punching capacity and punching capacity in  
335 experiment.

Test number	Wheel print (mm × mm)	$V_{exp}$ (kN)	$V_{R,c}$ (kN)	$V_{exp}/V_{R,c}$
BB1	200 × 200	348.7	141.9	2.458
BB2	200 × 200	321.4	141.9	2.266
BB7	200 × 200	345.9	141.9	2.438
BB19	115 × 150	317.8	121.6	2.613
FAT1S1	115 × 150	347.8	124.4	2.795
FAT7S1	115 × 150	393.7	127.4	3.091

336 **Table 6.** Determination of safety factor for deck of Van Brienenoord Bridge

Test number	$V_{exp}$ (kN)	$V_{BB}$ (kN)	$V_{BB,d}$ (kN)	$V_{Ed}$ (kN)	$V_{BB,d}/V_{Ed}$
BB1	348.7	1162.3	721.9	236.0	3.06
BB2	321.4	1071.3	665.4	236.0	2.82
BB7	345.9	1153.0	716.1	236.0	3.03
BB19	317.8	1059.3	658.0	232.0	2.84
FAT1S1	347.8	1159.3	720.1	232.0	3.10
FAT7S1	393.7	1312.3	815.1	232.0	3.51

337 *3.4. Assessment of case study bridge for fatigue*

338 The results of the experiments and the developed Wöhler curve can be interpreted for the  
339 assessment for fatigue. Given the geometry of the deck (see **Figure 1**), only two wheels (one of each  
340 axle) out of four wheels of the tandem can act on the deck together. The clear span is 2.1 m while the  
341 width of the design tandem is 2.4 m in total and 2.0 m center-to-center. For the interpretation of the  
342 test results, this means that the outcome of the tests with a double wheel print (Wöhler curve in  
343 **Figure 6b**) should be evaluated for the case study bridge for 250 million cycles, and that the outcome  
344 of the tests with a single wheel print (Wöhler curve in **Figure 6b**) should be evaluated for the case  
345 study bridge for 2 × 250 million cycles = 500 million cycles.

346 To use the Wöhler curves derived in the experiments for the assessment of the Van Brienenoord  
347 Bridge for fatigue, we will scale the fatigue load model to the 1:2 size of the test setup. Note that this  
348 approach differs from the assessment for punching, where we scaled up the capacity from the  
349 laboratory setup to the capacity of the case study bridge. Here, we use the opposite approach, to  
350 avoid having to change the Wöhler curve. The concentrated load of the fatigue load model is 105 kN.  
351 Scaling this load down to the 1:2 scale model uses a factor 2<sup>2</sup> = 4, so that the concentrated load becomes

352 26.25 kN. The distributed lane load of the fatigue load model is 3.105 kN/m<sup>2</sup>. For the 1:2 scale model,  
 353 the distributed lane load becomes 0.776 kN/m<sup>2</sup>.

354 In the 1:2 scale model, only concentrated loads are used, so the load that represents the  
 355 concentrated load as well as the distributed lane load should be determined. To determine the region  
 356 over which the distributed lane load should be considered, the cracking patterns in the experiments  
 357 were studied. The cracking pattern extends over 1.2 m for the experiments with a single wheel load  
 358 and over 2 m for the experiments with a double wheel load. To find the equivalent point load, we  
 359 determine first the bending moment caused by the distributed load, considering that the slab spans  
 360 over 1.8 m:

$$361 M_{dist,1wheel} = \frac{1}{8} \left( 0.776 \frac{\text{kN}}{\text{m}^2} \times 1.2\text{m} \right) (1.8\text{m})^2 = 0.38\text{kNm} \quad (22)$$

$$362 M_{dist,2wheel} = \frac{1}{8} \left( 0.776 \frac{\text{kN}}{\text{m}^2} \times 2\text{m} \right) (1.8\text{m})^2 = 0.63\text{kNm} \quad (23)$$

363 The equivalent concentrated load is then:

$$364 F_{eq} = \frac{4M_{dist}}{l_{span}} \quad (24)$$

365 which results in  $F_{eq} = 0.83$  kN for a single wheel load and  $F_{eq} = 1.40$  kN for a double wheel load. The  
 366 total load is then  $F = 27.08$  kN for a single wheel load and  $F = 27.65$  kN for a double wheel load.

367 The punching shear capacity of setup 2 is given in **Table 5** for FAT1S1 or cast 1 of the concrete  
 368 as 124.4 kN and for FAT7S1 or cast 2 as 127.4 kN according to the Eurocode punching provisions.  
 369 Recall that the design value of the enhancement factor is  $B_{Rd} = 1.622$ . As such, the design capacity of  
 370 the punching resistance with the punching perimeter around one wheel load, including the  
 371 enhancing effect of compressive membrane action becomes  $1.622 \times 124.4$  kN = 201.8 kN for the most  
 372 critical case (lowest capacity  $V_{Rd,c}$  as a result of the lowest concrete compressive strength). To  
 373 determine the capacity for punching with the case of a double wheel print, one could expect the  
 374 double capacity. However, the results in **Table 2** show that the capacity in the FAT8S2 is 1.64 times  
 375 the capacity in FAT7S1. This ratio is used for determining the punching shear capacity. The capacity  
 376 is now  $1.64 \times 201.8$  kN = 331.0 kN.

377 The load ratio can now be determined. For a single wheel load the load ratio is  $27.08$  kN / 201.8  
 378 kN = 0.134 and for a double wheel load the load ratio is  $2 \times 27.65$  kN / 331.0 kN = 0.167.

379 For the evaluation for one wheel load, Eq. (3) is used with  $N = 500$  million cycles. The resulting  
 380 ratio is then  $S_{char} = 0.348$ . For two wheel loads, using Eq. (5) with  $N = 250$  million cycles gives  $S_{char} =$   
 381 0.447. The outcome of the assessment is that the margin of safety for one wheel print is  $0.348 / 0.134$   
 382 = 2.60 or that inversely the UC = 0.39. For the case with two wheel prints, the margin of safety is  $0.447 / 0.167 = 2.68$  or inversely UC = 0.37. The results for one and two wheel prints are thus very similar.  
 383 The conclusion of the assessment is that based on the experimental results, we find that the case study  
 384 bridge fulfills the code requirements for fatigue.

#### 386 4. Discussion

387 In the previous two paragraphs, we calculated the Unity Checks for static punching ( $UC = 0.31$ ),  
 388 for fatigue punching of one wheel load after 500 million cycles of the single load ( $UC = 0.391$ ), and for  
 389 fatigue punching of two wheel loads after 250 million cycles of the axle ( $UC = 0.37$ ). Comparing these  
 390 Unity Checks leads to the conclusion that the most critical case is punching fatigue for a single wheel  
 391 load. The difference between the punching fatigue Unity Check for one and two wheel loads is  
 392 however negligible. In addition, the Unity Checks are small, and significantly smaller than the  
 393 limiting value of 1.0. This analysis shows the beneficial effect of taking into account compressive  
 394 membrane action.

395 All resulting Unity Checks are smaller than the limiting value of 1.0. This result means that the  
 396 code requirements for static and fatigue punching are met for the case study bridge. This outcome  
 397 directly shows the benefit of testing a scaled version of the Van Brienenoord Bridge in the laboratory.

398 In addition to the conclusion that the Van Brienenoord Bridge fulfills the code requirements for  
399 static and fatigue punching, we need to recall that this case study bridge was selected since it has the  
400 most critical geometry (largest span to depth ratio for the slab) of the existing slab-between-girder  
401 bridges in the Netherlands. As such, the conclusion becomes that all slab-between-girder bridges in  
402 the Netherlands, which form a well-defined subset of bridges in the Dutch bridge stock, fulfil the  
403 Eurocode requirements. Drawing this conclusion is valid, since these bridges were all built in the  
404 same time period, with the same materials, and same execution techniques – and are thus all very  
405 similar, with only small variations in the geometry and material properties.

406 One side note that we should place with the conclusion that all slab-between-girder bridges in  
407 the Netherlands fulfil the requirements for static and fatigue punching is that this conclusion is only  
408 valid for bridges without material degradation or other forms of damage. To ensure this premise,  
409 routine inspections remain necessary. Inspections are an important tool within the bridge  
410 management toolbox. When during an inspection indications of material degradation or damage are  
411 found, the bridge requires further analysis, and it should be evaluated if the conclusion that was  
412 based on an undamaged structure is still valid.

413 For this research, the outcome is twofold: 1) the small resulting Unity Checks based on the  
414 experimental results, and 2) the fact that with this approach the existing slab-between-girder bridges  
415 have been shown to fulfil the code requirements. This result also shows that constructing the 1:2 scale  
416 setups in the laboratory has been beneficial for the assessment of existing slab-between-girder  
417 bridges. While building a 1:2 scale bridge in the laboratory may be considered expensive and time-  
418 consuming, testing such a setup gives unique insights in the overall structural behavior of a structural  
419 system. Testing at the component level cannot provide such insights. Therefore, the cost-benefit  
420 analysis of these experiments is in favor of testing a structural system. Taking this approach is not  
421 common, but may become an interesting approach for ministries or departments of transportation  
422 when they are confronted with a problem for an entire category of bridges.

## 423 5. Conclusions

424 A number of existing slab-between-girder bridges in the Netherlands do not fulfil the  
425 requirements of the newly introduced Eurocodes when these are evaluated for punching (both static  
426 and for cycles of loading). The Eurocode model for determining the punching shear capacity is an  
427 empirical model, derived from the results of (mostly concentric) slab-column connection tests [40].  
428 The structural behavior of the thin slabs in slab-between-girder bridges is different from that of slab-  
429 column connections. In particular, the development of compressive membrane action increases the  
430 capacity significantly.

431 To study the structural behavior of slab-between-girder bridges, we selected as a case study the  
432 Van Brienenoord Bridge because it has the most critical slab geometry (largest span-to-depth ratio  
433 for the slabs) of this subset of bridges in the Dutch bridge stock. Based on the geometry of the case  
434 study bridge, we built two setups in the laboratory at 1:2 scale and carried out static and dynamic  
435 tests.

436 The outcome of the static tests can be used for assessing the static punching strength of the Van  
437 Brienenoord Bridge. Using the method given in the Eurocode for design by testing, a factor for  
438 converting mean values in design values of 1.53 is derived. Using this approach, the resulting Unity  
439 Check for punching shear of the Van Brienenoord Bridge becomes 0.31.

440 The outcome of the fatigue tests can be used to derive the Wöhler curve for thin slabs in slab-  
441 between-girder bridges. Analyzing the fatigue live load model, we select two critical loading cases  
442 for the fatigue assessment: the case with a single wheel load, and the case with two wheel loads (one  
443 of each axle). For both cases, we have the results of fatigue tests, and thus a Wöhler curve. The  
444 assessment is then carried out based on a service life of 100 years, which leads to 500 million cycles  
445 for the single wheel load and 250 million cycles for the double wheel load. Taking into account the  
446 factor to convert mean values to design values of 1.622 as derived from the static tests, we can then  
447 compare the applied load ratio to the load ratio resulting from the characteristic (5% lower bound)

448 Wöhler curve. Comparing these values gives a Unity Check of 0.39 for the case with a single wheel  
 449 print and of 0.37 for the case with a double wheel print.

450 Evaluating the results of the Unity Checks, we can identify the most critical case, which is (by a  
 451 small margin) the case of fatigue punching under a single wheel load. The resulting Unity Checks are  
 452 however much smaller than the limiting value of 1.0. As such, the conclusion is that the Van  
 453 Brienenoord Bridge fulfils the Eurocode requirements for static punching and fatigue. Since the case  
 454 study bridge is selected based on the most critical geometry, we can say that by extent all other slab-  
 455 between-girder bridges in the Netherlands fulfil the Eurocode requirements for static and fatigue  
 456 punching. This final conclusion, however, is only valid for bridges without deterioration and material  
 457 degradation. Routine inspections remain an important bridge management tool to identify bridges  
 458 that require further study.

459 **List of notations**

460 $b$	width
461 $c$	concrete cover
462 $d$	average effective depth
463 $d_l$	effective depth to the longitudinal reinforcement
464 $d_t$	effective depth to the transverse reinforcement
465 $f_{ck,cube}$	characteristic cube concrete compressive strength
466 $f_{cm,cube}$	average cube concrete compressive strength
467 $f_{ck}$	characteristic cylinder concrete compressive strength
468 $f_{cm}$	average cylinder concrete compressive strength
469 $h$	height
470 $k$	size effect factor
471 $k_1$	factor on effect of axial stresses
472 $l$	length
473 $l_{span}$	span length
474 $q_{ik}$	distributed lane load
475 $u$	punching perimeter length
476 $v_{min}$	lower bound of shear capacity
477 $v_{R,c}$	mean capacity for punching shear
478 $v_{Rd,c}$	design capacity for punching shear
479 $A_{s,l}$	longitudinal reinforcement area
480 $A_{sp}$	area of prestressing steel
481 $A_{s,t}$	transverse reinforcement area
482 $A_u$	area within punching perimeter
483 $B_{Rd}$	design capacity derived from statistical results of experiments
484 $COV$	coefficient of variation
485 $C_{Rd,c}$	constant in punching capacity equation
486 $DL$	dead load
487 $DW$	superimposed dead load
488 $F$	applied load
489 $F_{eq}$	equivalent load
490 $LL$	live load
491 $M_{dist,1wheel}$	bending moment caused by distributed lane load for influence area of one wheel load
492 $M_{dist,2wheel}$	bending moment caused by distributed lane load for influence area of two wheel loads
493 $N$	number of cycles
494 $P_{max}$	load at failure
495 $Q_{ik}$	axle load of design tandem
496 $S$	load ratio
497 $S_{char}$	characteristic value of load ratio (5% lower bound Wöhler curve)
498 $U$	load combination

499	$UC$	Unity Check
500	$V_{BB}$	average capacity of deck of Van Brienenoord Bridge based on experiments
501	$V_{BB,d}$	design capacity of deck of Van Brienenoord Bridge based on experiments
502	$V_{R,c}$	mean value of the punching shear capacity
503	$V_{Rd,c}$	design value of the punching shear capacity
504	$V_{Ed}$	design value of punching shear demand
505	$V_{exp}$	experimental punching capacity
506	$\alpha$	factor that considered effect of experiments
507	$\alpha_{qi}$	factor on distributed lane loads
508	$\alpha_{Qi}$	factor on design tandem
509	$\beta$	reliability index
510	$\gamma_T$	partial factor derived from experiments
511	$\mu$	mean value of experimental results
512	$\rho_{avg}$	average reinforcement ratio
513	$\rho_l$	longitudinal reinforcement ratio
514	$\rho_t$	transverse reinforcement ratio
515	$\sigma_{cp}$	average axial stress
516	$\sigma_{cx}$	longitudinal axial stress
517	$\sigma_{cy}$	transverse axial stress

518 **Author Contributions:** conceptualization, CV and HS; methodology, CV, RK and EL; validation, EL; formal  
519 analysis, RK and EL; investigation, RK and CV; resources, HS; data curation, EL and RK; writing—original draft  
520 preparation, EL; writing—review and editing, RK, CV and HS; visualization, RK and EL; supervision, CV and  
521 HS; project administration, CV and HS; funding acquisition, CV.

522 **Funding:** This research was funded by Rijkswaterstaat, Ministry of Infrastructure and the Environment. The  
523 APC was funded by Delft University of Technology.

524 **Acknowledgments:** The authors wish to express their gratitude and sincere appreciation to the Dutch Ministry  
525 of Infrastructure and the Environment (Rijkswaterstaat) for financing this research work. We are deeply  
526 indebted to our colleague Albert Bosman for his work in the laboratory and the meticulous reporting of the first  
527 series of experiments. We'd also like to thank our former colleagues Sana Amir and Patrick van Hemert for their  
528 contributions to the beginning of the experimental work.

529 **Conflicts of Interest:** The authors declare no conflict of interest. The funders had no role in the design of the  
530 study; in the collection and analyses of data. The funders were involved with the practical interpretation of the  
531 data, writing of the manuscript, and decision to publish the results.

## 532 References

- 533 1. CEN. Eurocode 1: Actions on structures - Part 2: Traffic loads on bridges, NEN-EN 1991-2:2003. Comité  
534 Européen de Normalisation: Brussels, Belgium, 2003; p 168.
- 535 2. Code Committee 351001. *NEN 6720 Technical Foundations for Building Codes, Concrete provisions TGB 1990 -*  
536 *Structural requirements and calculation methods (VBC 1995)* (in Dutch); Civil engineering center for research and  
537 regulation, Dutch Normalization Institute: Delft, The Netherlands, 1995; pp. 245.
- 538 3. CEN. Eurocode 2: Design of Concrete Structures - Part 1-1 General Rules and Rules for Buildings. NEN-  
539 EN 1992-1-1:2005. Comité Européen de Normalisation: Brussels, Belgium, 2005; p 229.
- 540 4. Lantsoght, E.O.L.; van der Veen, C.; de Boer, A.; Walraven, J.C. Recommendations for the Shear Assessment  
541 of Reinforced Concrete Slab Bridges from Experiments *Structural Engineering International* **2013**, *23*, 418-426.
- 542 5. Amir, S.; Van der Veen, C.; Walraven, J.C.; de Boer, A. Experiments on Punching Shear Behavior of  
543 Prestressed Concrete Bridge Decks. *Aci Structural Journal* **2016**, *113*, 627-636.
- 544 6. Teworte, F.; Herbrand, M.; Hegger, J. Structural Assessment of Concrete Bridges in Germany — Shear  
545 Resistance under Static and Fatigue Loading. *Structural Engineering International* **2015**, *25*, 266-274.
- 546 7. Bagge, N.; Nilimaa, J.; Puurula, A.; Täljsten, B.; Blanksvärd, T.; Sas, G.; Elfgren, L.; Carolin, A. Full-Scale  
547 Tests to Failure Compared to Assessments – Three Concrete Bridges. In Proceedings of fib symposium 2017,  
548 Maastricht, the Netherlands.
- 549 8. Brühwiler, E.; Vogel, T.; Lang, T.; Luechinger, P. Swiss Standards for Existing Structures. *Structural*  
550 *Engineering International* **2012**, *22*, 275-280, doi:10.2749/101686612x13291382991209.

551 9. Kong, J.S.; Frangopol, D.M. Probabilistic optimization of aging structures considering maintenance and  
552 failure costs. *Journal of Structural Engineering-Asce* **2005**, *131*, 600-616, doi:10.1061/(asce)0733-  
553 9445(2005)131:4(600).

554 10. Frangopol, D.M.; Sabatino, S.; Dong, Y. Bridge Life-Cycle Performance and Cost: Analysis, Prediction,  
555 Optimization and Decision Making. In Proceedings of Maintenance, Monitoring, Safety, Risk and Resilience of  
556 Bridges and Bridge Networks, Foz do Iguacu, Brazil; pp. 2-20.

557 11. Vergoossen, R.; Naaktgeboren, M.; 't Hart, M.; De Boer, A.; Van Vugt, E. Quick Scan on Shear in Existing  
558 Slab Type Viaducts. In Proceedings of International IABSE Conference, Assessment, Upgrading and  
559 Refurbishment of Infrastructures, Rotterdam, The Netherlands; p. 8.

560 12. Lantsoght, E.O.L.; van der Veen, C.; de Boer, A.; Walraven, J. Using Eurocodes and AASHTO for assessing  
561 shear in slab bridges. *Proceedings of the Institution of Civil Engineers – Bridge Engineering* **2016**, *169*, 285-297.

562 13. Amir, S. Compressive Membrane Action in Prestressed Concrete Deck Slabs. PhD Thesis. Delft University  
563 of Technology, 2014.

564 14. Collings, D.; Sagaseta, J. A review of arching and compressive membrane action in concrete bridges.  
565 *Institution of Civil Engineers – Bridge Engineering* **2015**, *169*, 271-284.

566 15. Eyre, J.R. Direct assessment of safe strengths of RC slabs under membrane action. *Journal of Structural  
567 Engineering-Asce* **1997**, *123*, 1331-1338.

568 16. Highways Agency. *Corrections within design manual for roads and bridges, use of compressive membrane action  
569 in bridge decks*; London, United Kingdom, 2007; pp 35-51.

570 17. Kirkpatrick, J.; Rankin, G.I.B.; Long, A.E. The influence of compressive membrane action on the  
571 serviceability of beam and slab bridge decks. *The structural engineer* **1986**, *64B*, 6-9.

572 18. Kuang, J.S.; Morley, C.T. A Plasticity Model for Punching Shear of Laterally Restrained Slabs with  
573 Compressive Membrane Action. *International Journal of Mechanical Sciences* **1993**, *35*, 371-385.

574 19. Tong, P.Y.; de V. Batchelor, B. Compressive membrane enhancement in two-way bridge slabs. *SP* **30-12**  
575 **1972**, 271-286.

576 20. Hewitt, B.E.; de Batchelor, B.V. Punching shear strength of restrained slabs. *Journal of the Structural Division*  
577 **1975**, *101*, 1837-1853.

578 21. Lantsoght, E.O.L.; Van der Veen, C.; R.T. Koekkoek; Sliedrecht, H. Capacity of prestressed concrete bridge  
579 decks under fatigue loading. In Proceedings of fib symposium 2019, Cracow, Poland.

580 22. Bennett, E.W.; Muir, S.E.S.J. Some fatigue tests of high-strength concrete in axial compression. *Magazine of  
581 Concrete Research* **1967**, *19*, 113-117.

582 23. Lantsoght, E.O.L.; van der Veen, C.; de Boer, A. Proposal for the fatigue strength of concrete under cycles  
583 of compression. *Construction and Building Materials* **2016**, *107*, 138-156.

584 24. Isojeh, B.; El-Zeghayar, M.; Vecchio, F.J. Fatigue Resistance of Steel Fiber-Reinforced Concrete Deep Beams.  
585 *ACI Structural Journal* **2017**, *114*, doi:10.14359/51700792.

586 25. Teng, S.; Ma, W.; Tan, K.H.; Kong, F.K. Fatigue tests of reinforced concrete deep beams. *The structural  
587 engineer* **1998**, *76*, 347-352.

588 26. Teworte, F.; Hegger, J. Shear Fatigue of Prestressed Concrete Beams. In Proceedings of IABSE 2011; p. 8.

589 27. Muller, J.F.; Dux, P.F. Fatigue of Prestressed Concrete Beams with Inclined Strands. *Journal of Structural  
590 Engineering* **1994**, *120*, 1122-1139, doi:doi:10.1061/(ASCE)0733-9445(1994)120:4(1122).

591 28. Yuan, M.; Yan, D.; Zhong, H.; Liu, Y. Experimental investigation of high-cycle fatigue behavior for  
592 prestressed concrete box-girders. *Construction and Building Materials* **2017**, *157*, 424-437,  
593 doi:<https://doi.org/10.1016/j.conbuildmat.2017.09.131>.

594 29. Fujiyama, C.; Gebreyouhannes, E.; Maekawa, K. Present Achievement and Future Possibility of Fatigue  
595 Life Simulation Technology for RC Bridge Deck Slabs. *Society for Social Management Systems Internet Journal* **2008**,  
596 4.

597 30. Harajli, M.H.; Naaman, A.E. Static and Fatigue Tests on Partially Prestressed Beams. *Journal of Structural  
598 Engineering* **1985**, *111*, 1602-1618, doi:doi:10.1061/(ASCE)0733-9445(1985)111:7(1602).

599 31. Xin, Q.; Dou, Y.; Chen, W. *Load Spectrum and Fatigue Life Computer Analysis of Prestressed Concrete Bridges*;  
600 2015; Vol. 9, pp. 247-266.

601 32. Rijkswaterstaat. Guidelines Assessment Bridges - assessment of structural safety of an existing bridge at  
602 reconstruction, usage and disapproval (in Dutch), RTD 1006:2013 1.1. Utrecht, the Netherlands, 2013; p 117.

603 33. Van der Veen, C.; Bosman, A. *Vermoeiingssterkte voorgespannen tussenstort*; Stevin Report nr. 25.5-14-06,  
604 Delft University of Technology, Delft, the Netherlands. 2014; p 65.

605 34. Lantsoght, E.O.L.; Van der Veen, C.; Koekkoek, R.T.; Sliedrecht, H. Fatigue testing of transversely  
606 prestressed concrete decks. *ACI Structural Journal* **in press**.

607 35. Koekkoek, R.T.; van der Veen, C.; de Boer, A. Fatigue Tests on Post-tensioned Bridge Decks. *fib Symposium  
608 2017*, Maastricht, the Netherlands; pp. 912-920.

609 36. Koekkoek, R.T.; van der Veen, C. *Measurement Report Fatigue Tests on Slabs Cast In-Between Prestressed*  
610 *Concrete Beams*; Stevin Report nr. 25.5-17-14, Delft University of Technology, Delft, the Netherlands. 2017; p 196.

611 37. Lantsoght, E.O.L.; Van der Veen, C.; Koekkoek, R.T.; Sliedrecht, H. Punching capacity of prestressed  
612 concrete bridge decks under fatigue. *ACI Structural Journal* **in press**.

613 38. Code Committee 351001. *Assesment of structural safety of an existing structure at repair or unfit for use - Basic*  
614 *Requirements*, NEN 8700:2011 (in Dutch); Civil center for the execution of research and standard, Dutch  
615 Normalisation Institute: Delft, The Netherlands, 2011; pp. 56.

616 39. CEN. Eurocode – Basis of structural design, NEN-EN 1990:2002 Comité Européen de Normalisation:  
617 Brussels, Belgium, 2002; p 103.

618 40. Walraven, J.C. *Background document for EC-2, Chapter 6.4 Punching Shear*; Stevin Report Nr. 25.5-02-37. Delft  
619 University of Technology: Delft, The Netherlands, 2002; pp 1-16.

620

621

622